ELSEVIER

International Journal of Mass Spectrometry 210/211 (2001) 265–281

International Journal of Mass Spectrometry

www.elsevier.com/locate/ijms

$Fe(CH_4)_n^+$ and $Ni(CH_4)_n^+$ clusters: experimental and theoretical bond energies for $n = 1–6$

Qiang Zhang, Paul R. Kemper, Michael T. Bowers*

Department of Chemistry, University of California, Santa Barbara, California 93106-9510, USA

Received 15 November 2000; accepted 16 January 2001

Abstract

Measurements are reported for sequential clustering of CH_4 to Fe^+ and Ni^+ ions under equilibrium conditions. Detailed density functional theory calculations were performed to provide structural and electronic configuration information and to help analyse and interpret the experimental data. The calculations indicate that the first two CH_4 ligands add on opposite sides of the Fe^+ core ion in an η^3 configuration, in an η^2 configuration for Ni^+, and induce significant *s/d* hybridization on both of the metal centers. This hybridization both reduces Pauli repulsion and fosters sigma donation from the ligands into the 4*s* orbital on M^+. Another major covalent interaction is the donation from CH_4 into the singly occupied *d* orbital(s) on M^+ for both η^2 and η^3 configurations. For Fe^+, the change of spin state, from ^6D ($3d^64s^1$) to ^4F ($3d^7$), takes place during the clustering of the first methane ligand. The clustering of the third CH_4 to Fe^+ and Ni^+, unlike $Co^+(CH_4)_3$, is not impeded by the *s/d* hybridization present for $n = 1$ and 2. The interactions of all three CH_4 ligands with the Fe^+ and Ni^+ core are essentially the same. The *m/z* 120 peak [nominally $Fe^+(CH_4)_4$] and the *m/z* 122 peak [nominally $Ni^+(CH_4)_4$] were formed irreversible in the temperature range from 270 to 170 K, probably due to the persistent impurity we reported earlier for the Co^+ system. The $n = 5$ and 6 ligands are very weakly bound and begin a second solvation shell. Calculations suggest the $n = 6$ cluster forms a pseudo octahedral complex. (Int J Mass Spectrom 210/211 (2001) 265–281) © 2001 Elsevier Science B.V.

Introduction

Sigma bond activation by transition metal centers has long been a central focus in inorganic chemistry. Conventional wisdom is that neutral first row transition metal atoms are usually unreactive due to the doubly occupied, repulsive 4*s* orbital or due to the half filled 3*d* and 4*s* shells of Cr and Cu [1]. Hence "activating" ligands need to be added to oxidize the metals to d^n configurations. This is especially true for activation of "inert" systems like saturated hydrocarbons, where controlled activation has tremendous technological importance [2]. Although much success has been achieved in these studies, the addition of often bulky ligands makes high level ab initio calculations extremely difficult. As a consequence, the details of the activation mechanism are not yet well known.

Our approach has been to start with transition metal atoms in their first oxidation states; that is singly charged ions. One immediate advantage is that all first row transition metal centers have either $3d^n$ or $3d^{n-1}\,4s^1$ configurations and thus intrinsically more reactive than their neutral analogues. The second advantage is charged species are easy to manipulate

* Corresponding author. E-mail: bowers@chem.ucsb.edu

PII S1387-3806(01)00402-X

and the powerful methods of mass spectroscopy can be applied. A variety of methods has been developed to study the energetics and mechanism of transition metal ions reacting with a wide range of neutrals [3]. Of direct relevance to the work discussed here are equilibrium measurements, initiated by Paul Kebarle many years ago [4]. and guided ion beam measurements developed by Armentrout [5] that obtain bond energies using collision induced dissociation. Careful systematic measurements of M^+–L bond energies offer excellent opportunities for understanding sigma bond activation, especially when coupled with theory [6].

The initial targets of our groups were first row metal ions sequentially adding dihydrogen [7]. Careful measurements of bond energies were coupled with high level calculations to yield both structural information and details of the nature of the bonding. It rapidly became apparent that the idea that the bonding was primarily electrostatic was incorrect. For example, for $M^+(H_2)_3$ systems Ti, Mn, and Zn form ~90° angles between ligands, Cr, Ni, and Cu have planar D_{3h} complexes, and Fe, Co, and V form T-shaped C_{2v} complexes [8]. From the systematic study four factors that influence the bonding are, in order of importance: [8].

(1) backbonding from filled d_π orbitals on the metal to σ^* orbitals on H_2; (2) sigma donation from H_2 into (partially) empty d_σ or especially *s* orbitals on M^+; (3) repulsion from a (partially) filled d_σ or *s* orbital on M^+; and (4) electrostatic attraction between M^+ and the H_2 ligands.

When the *s* orbital on M^+ is occupied, factor (3) becomes dominant [9]. Most importantly, these factors really became apparent only after a systematic study of the entire first row was completed. In this article we are continuing a new systematic study of bonding between first row metal ions and CH_4. In our initial study we determined Ti^+ activated methane on the addition of the third CH_4 ligand [10], eliminated H_2, and appeared to generate an olefin ligand with subsequent CH_4 addition. Among the late metals, Co^+ was found to sequentially add CH_4 through $n = 6$ with no H_2 elimination or C–H bond insertion [11,12]. When the cyclopentadienyl (Cp) ligand was added to Co^+, however, H_2 elimination was observed on addition of the second CH_4 ligand with active involvement of the Cp ring [13].

In this article we report the results of CH_4 clustering with Fe^+ and Ni^+, metals that fall on either side of cobalt. The Fe^+ system has been investigated before using guided ion beam methods [14] where it was reported that up to four CH_4 ligands are strongly bound to the metal center. This contrasts with the Co^+ system where only two CH_4 ligands were strongly bound. It was suggested a spin change on the Fe^+ center was responsible, and occurred on addition of the second and fourth CH_4 molecules. On the other hand the Ni^+ system has not yet been studied and it could prove interesting as the bonding in $Ni^+(H_2)_n$ was significantly different than found in $Fe^+(H_2)_n$ and $Co^+(H_2)_n$ for $n \geq 3$.

2. Experimental methods

Experimental details of the method and instrument have been given previously [15–17]. The Fe^+ and Ni^+ ions were formed by electron impact or surface ionization on $Fe(CO)_5$ and $Ni(CO)_4$, respectively. The transition metal ions, M^+, were mass selected by a quadrupole mass filter and injected into a drift cell containing the CH_4 reaction gas (typical pressures 1–5 Torr). The ions drift under a weak electric field that does not measurably perturb their thermal energies and rapidly come to equilibrium:

$$M^+(CH_4)_{n-1} + CH_4 \rightleftharpoons M^+(CH_4)_n \quad (1)$$

The cell temperature is variable from 80 to 800 K and equilibrium constants were measured over this range.

$$K = \frac{M^+(CH_4)_n\,(760)}{M^+(CH_4)_{n-1}\,P_{CH_4}} \quad (2)$$

where P_{CH_4} is the pressure of CH_4 in Torr, (760) Torr normalizes to standard state conditions and $M^+(CH_4)_n$, $M^+(CH_4)_{n-1}$ are the measured intensities of the ions. The standard state free energy is then calculated

$$\Delta G_T^0 = -RT \ln K \quad (3)$$

and enthalpies and entropies determined by plotting ΔG_T^0 versus T:

$$\Delta G_T^0 = \Delta H_T^0 - T\Delta S_T^0 \quad (4)$$

where ΔH_T^0 and ΔS_T^0 are the intercept and slope of the plot, respectively. These quantities are valid over the temperature range of the experiment. To get true bond dissociation energies (ΔH_0^0), extrapolations using statistical mechanics methods and theoretically determined structures and vibrational frequencies are accomplished.

Theoretical methods

All calculations were carried out at the density functional theory (DFT) level using the unrestricted open shell Becke-style 3 parameter using the Lee-Yang-Parr correlation functional (B3LYP) functional [18,19] with the GAUSSIAN98 program package [20]. For carbon and hydrogen, the 6-31G(*d,p*) basis was used. For transition metals, two basis sets were used to ensure basis set superposition error was minimized. First, we used the double zeta valence polarization (DZVP) basis set [21], which is a [5*s*3*p*2*d*] contraction of (15*s*9*p*5*d*) primitive set. This basis leads to imaginary frequency problems for the weak M^+–CH_4 clustering modes whereas restricting the molecules to high symmetry, i.e. C_{2v} or C_{3v}. After lifting the symmetry restriction, the molecules converged to a geometry with C_s symmetry which lies between C_{2v} and C_{3v}. Consequently, we used the (14*s*9*p*5*d*)[8*s*4*p*3*d*] Wachters basis augmented with two diffuse *p* functions, one diffuse *d* function and a (3*f*)[1*f*] polarization function [22,23], which result in a (14*s*11*p*6*d*3*f*)[8*s*6*p*4*d*1*f*] basis set. The imaginary frequency problem is essentially fixed with this basis set. Even after breaking the symmetry restriction, the molecules still favor and converge to high symmetry structures, i.e. C_{2v} or C_{3v} for M^+–CH_4. The minimum energy structure achieved with the DZVP basis set is far away from that predicted with the Wachters basis set, with the hydrogens rotated 30° from the M^+–C axis. The possible reason for this significant difference is that the DZVP basis is insufficient to accurately deal with the shallow potential well in which the C–H bonds of CH_4 rotate relative to the metal center.

For iron ion, $^6D(3d^6\ 4s^1)$ is the ground state. The *j*-averaged first excited state, $^4F(3d^7)$, lies 5.7 kcal/mol higher in energy [24]. However, the DFT calculation with a B3LYP functional erroneously predicts the electronic ground state of Fe^+ to be $^4F(3d^7)$, lower than the $^6D(3d^6\ 4s^1)$ state by 3.5 kcal/mol with a Wachters(*f*) basis in our present calculation and by 3.2 kcal/mol in the calculation by Koch and co-worker [25]. This error of 9.2 kcal/mol reflects a "well-known" problem in DFT, i.e the bias toward d^n over $d^{n-1}s^1$ configurations [26]. Fortunately, for d^7 confi gurations the change of 3*d*, electron population is minor: the lowest one is 6.85 for $Fe^+(CH_4)$ (C_{2v}, $^4A_1$) and the highest one is 7.16 for $Fe^+(CH_4)_6$ (D_{2h}, $^4B_{3g}$). The increase of 3*d* electron population with increasing cluster size is believed due to electron donation from the methane ligands into the half filled 3*d* orbitals of iron. Therefore, to calibrate the state separation error we simply correct the energy splitting by the Mulliken 3*d* electron population of iron for the first cluster only. In the $Fe^+(CH_4)$ (C_{2v}, $^4A_1$ state), for example such calibration will increase the diabatic bond dissociation energy by 1.4 kcal/mol. The uncertainty is about 10% and relatively small compared to the total bond dissociation energy. For Ni^+, the calculated 26.6 kcal/mol $^2D(3d^9) \rightarrow {}^4F(3d^8\ 4s^1)$ energy separation with the Wachters(*f*) basis is very close to the experimental 25.0 kcal/mol splitting. No energy separation calibration was performed for $Ni^+(CH_4)_n$ clusters. With the DZVP basis, the energy separation error is 16.0 kcal/mol for Fe^+ and 6.5 kcal/mol for Ni^+, which is much larger than that with the Wachters(*f*) basis set. Full geometry optimization and frequency analyses are performed on all $M^+(CH_4)_n$ clusters using the augmented Wachters basis set.

4. Results and discussion

The experimental data are plotted in Figs. 1 and 2 as ΔG_T^0 versus temperature graphs. A summary of the experimental and theoretical enthalpies and experimental entropies for the M^+/CH_4 association reac-

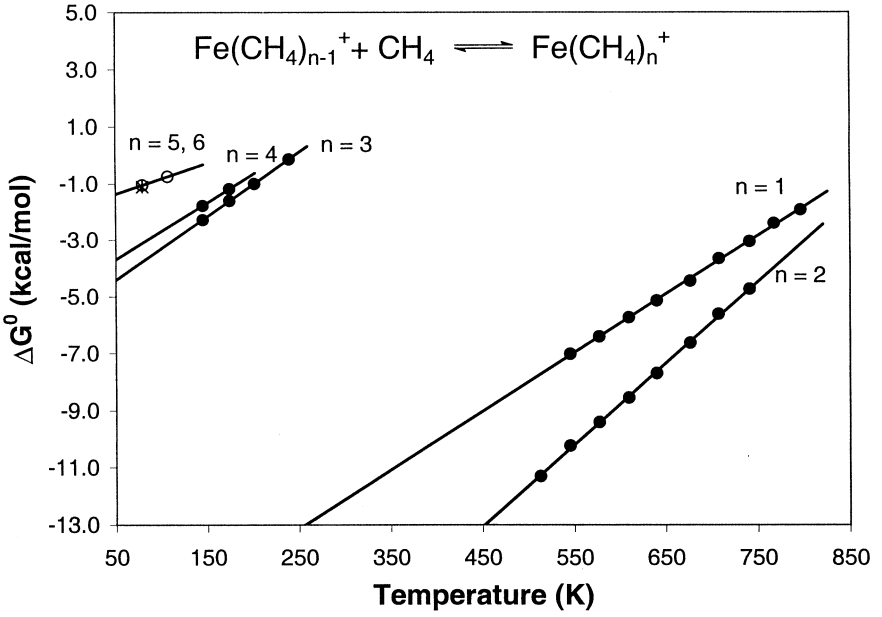

Fig. 1. Plot of experiment ΔG_T^0 values vs. temperature for sequential clustering of CH_4 ligands to Fe^+. The $n = 5$ data are the open circle and the $n = 6$ data point is the asterisk.

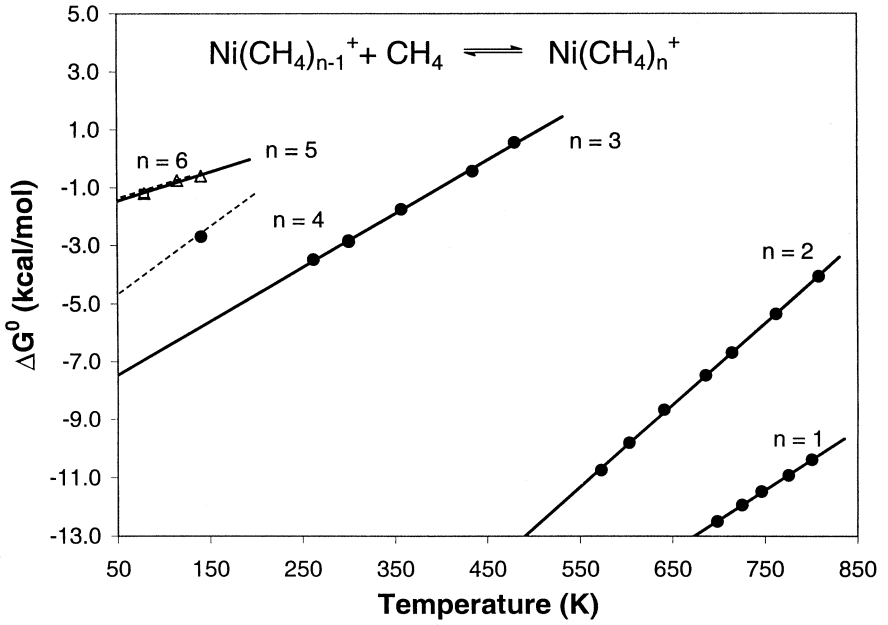

Fig. 2. Plot of experimental ΔG_T^0 values vs. temperature for sequential clustering of CH_4 ligands to Ni^+. The $n = 5$ data are the open circle (△) and the $n = 6$ data point is the asterisk. For $n = 4$ only a single data point could be obtained (see text). The dashed lines assume $\Delta S_T^0 = -20$ cal/mol K) for $n = 4$ and -10 cal/(mol K) for $n = 6$.

Table 1
Experimental results for the reactions $Fe^+(CH_4)_{n-1} + CH_4 \rightleftharpoons Fe^+(CH_4)_n$ for $n = 1$–6

	Experiment				Theory			
Ion	BDE (D_0) (kcal/mol)	$-\Delta H_T^{0a}$ (kcal/mol)	$-\Delta S_T^0$ (cal mol^{-1} K^{-1})	T (K)	Symmetry	D_e^b (kcal/mol)	D_e^c (kcal/mol)	D_0^c (kcal/mol)
$Fe^+(CH_4)$	17.5	18.3 (13.7)[d]	20.6	670 ± 130	$C_{3v}(z)$ (^4E)	16.2	15.2	15.5
					$C_{2v}(x)$ ($^4A_2$)	15.0	15.2	15.1
					$C_{2v}(z)$ ($^4A_1$	14.4	14.0	13.7
					$C_{3v}(z)$ (^6E)	10.8	10.4	10.4
					$C_{2v}(z)$ ($^6A_1$)	9.5	9.4	9.5
$Fe^+(CH_4)_2$	26.0	25.9 (23.3)[d]	28.6	625 ± 125	$D_{3d}(z)$ (^4E_g)	21.3	22.0	21.5
					$D_{2h}(x)$ ($^4B_{1g}$)	19.2	21.3	19.6
					$D_{2h}(z)$ (^4A_g)	18.4	20.1	19.0
$Fe^+(CH_4)_3$	5.2	5.6 (23.6)[d]	22.5	190 ± 50	$C_{2v}(x)$ ($^4A_2$)	5.8	6.6	4.0
					$C_{2v}(z)$ ($^4A_1$)	3.8		
					$D_{3d}(z)$ (^4E)	2.1		
$Fe^+(CH_4)_4$	~4.9	~4.7 (17.6)[d]	~20	160 ± 15	$D_{4h}(z)$ ($^4B_{2g}$)	4.1	4.1	3.0
					$D_{2d}(z)$ ($^4A_1$)	2.7	3.4	2.8
$Fe^+(CH_4)_5$		~2	~10	95 ± 15	$C_{2v}(z)$ ($^4A_2$)	0.8	0.5	
$Fe^+(CH_4)_6$		~2	~10	80	$D_{2h}(z)$ ($^4B_{1g}$)	0.8	0.2	

[a]Estimated uncertainty of 1%–2%.
[b]Calculated from DZVP basis set.
[c]Calculated from Wachters(*f*) basis.
[d]See [14].

Table 2
Experimental results for the reactions $Ni^+(CH_4)_{n-1} + CH_4 \rightleftharpoons Ni^+(CH_4)_n$ for $n = 1$–6

	Experiment				Theory			
Ion	BDE (D_0) (kcal/mol)	$-\Delta H_T^{0a}$ (kcal/mol)	$-\Delta S_T^{0a}$ (cal mol^{-1} K^{-1})	T (K)	Symmetry	D_e^b (kcal/mol)	D_e^c (kcal/mol)	D_0^c (kcal/mol)
$Ni^+(CH_4)$	24.9	26.8	20.5	750 ± 50	$C_{2v}(x)$ ($^2A_2$)	24.2	23.8	23.9
					$C_{2v}(z)$ ($^2A_2$)	23.6	22.6	22.5
$Ni^+(CH_4)_2$	26.5	26.8	28.2	690 ± 110	$D_{2h}(x)$ ($^2B_{1g}$)	23.6	24.2	22.9
					$D_{2h}(z)$ ($^2B_{1g}$)	21.9	21.3	20.4
$Ni^+(CH_4)_3$	9.3	8.4	18.5	350 ± 100	C_{2v})(x) ($^2A_1$)	8.6	8.1	7.4
					C_{2v})(x) ($^2A_2$)	8.5	8.5	7.4
					$C_{2v}(z)$ ($^2A_2$)[d]	3.8	2.0	
					$C_{2v}(z)$ ($^2A_2$)[e]	3.3	1.9	
$Ni^+(CH_4)_4$	~5.5	~5.5	~20	140	$D_{4h}(z)$ ($^2B_{2g}$)	6.8	4.9	3.7
					C_s	2.8	−0.5	
$Ni^+(CH_4)_5$	~2.0	2.0	9.9	110 ± 30	$C_{2v}(z)$ ($^2A_1$)	1.6	0.5	
$Ni^+(CH_4)_6$	~2.0	~2.0	~10	80	$D_{2h}(z)$ (^2A_g)	0.9	0.4	

[a]Estimated uncertainty of 1%–2%.
[b]Calculated from DZVP basis set.
[c]Calculated from Wachters(*f*) basis.
[d]See Fig. 6 (c).
[e]See Fig. 6 (d).

Table 3
Natural bond orbital population of Fe^+ in $Fe^+(CH_4)_n$ clusters

Cluster	State	4*s*	$4p_x$	$4p_y$	$4p_z$	d_{xy}	d_{xz}	d_{yz}	$d_{x^2-y^2}$	d_{z^2}
$Fe^+(CH_4)$	η^3 $C_{3v}(z)$ ^4E	0.1663	0.0039	0.0039	0.0011	1.9949	1.0160	1.0152	0.9996	1.8407
	η^2 $C_{2v}(x)$ $^4A_2$	0.0947	0.0012	0.0038	0.0022	1.9908	1.0000	1.0161	0.9997	1.9376
	η^2 $C_{2v}(z)$ $^4A_1$	0.1887	0.0012	0.0022	0.0039	1.0000	1.0007	1.0159	1.9927	1.8455
	η^3 $C_{3v}(z)$ ^6E	1.0105	0.0032	0.0032	0.0085	1.0000	1.0073	1.0107	1.9964	1.0160
	η^2 $C_{2v}(z)$ $^6A_1$	1.0186	0.0011	0.0022	0.0147	1.0000	1.0013	1.0090	1.9969	1.0209
$Fe^+(CH_4)_2$	η^3 $D_{3d}(z)$ ^4E_g	0.2957	0.0057	0.0057	0.0014	1.9930	1.0345	1.0321	0.9997	1.7784
	η^2 $D_{2h}(x)$ $^4B_{1g}$	0.2208	0.0072	0.0017	0.0033	1.9843	1.0369	1.0000	1.0029	1.8855
	η^2 $D_{2h}(z)$ ^4A_g	0.3348	0.0075	0.0034	0.0016	1.0371	1.0024	1.0000	1.8297	1.9464
$Fe^+(CH_4)_3$	η^2 $C_{2v}(x)$ $^4A_2$	0.1867	0.0073	0.0059	0.0037	1.9777	1.0350	1.0150	1.0424	1.9112
$Fe^+(CH_4)_4$	η^2 $D_{4h}(z)$ $^4B_{2g}$	0.1769	0.0083	0.0083	0.0034	1.9857	1.0298	1.0298	1.0735	1.9286
	η^2 $D_{2d}(z)$ $^4A_1$	0.1310	0.0071	0.0071	0.0093	1.0290	1.0489	1.0489	1.9781	1.9685
$Fe^+(CH_4)_5$	η^2 $C_{2v}(z)$ $^4A_2$	0.1708	0.0087	0.0087	0.0042	1.9856	1.0301	1.0292	1.0717	1.9315
$Fe^+(CH_4)_6$	η^2 $D_{2h}(z)$ $^4B_{1g}$	0.1700	0.0045	0.0091	0.0092	1.0284	1.0295	1.9857	1.7162	1.2889

tions is given in Tables 1 and 2. The ΔS_T^0 and ΔH_T^0 values are taken from slopes and intercepts, respectively, of linear fits to the ΔG_T^0 versus temperature plots [15,16]. The bond energies at 0 K (ΔH_0^0) was derived from statistical mechanical fitting as described earlier. The natural bond orbital (NBO) populations for the Fe^+ and Ni^+ 3*d*/4*s* orbitals are listed in Tables 3 and 4. The B3LYP optimized geometries with Wachters(*f*)/6-31G(*d*, *p*) basis for the successive clustering of CH_4 to Fe^+ and Ni^+ are displayed in Figs. 3–7.

On a global basis, good agreement is found between the theoretical and experimental bond dissociation energies (BDES) for $n = 1–6$ for Fe^+, Co^+, and Ni^+. In particular, the first two CH_4 ligands are theoretically predicated to be relatively strongly bound as observed. The BDEs for the third and the fourth clusters, while still substantial, are 15 kcal/mol or so weaker than the first two, which is also in good agreement with the theory. For $n = 5$ and 6, the theory indicates a bond dissociation energy of about 0.5 kcal/mol and a bond length of about 4 Å. These BDE and the geometry information support the second solvation shell structure suggested by experiment for these ligands. In the

Table 4
Natural bond orbital population of Ni^+ in $Ni^+(CH_4)_n$ clusters

Cluster	State	4*s*	$4p_x$	$4p_y$	$4p_z$	d_{xy}	d_{xz}	d_{yz}	$d_{x^2-y^2}$	d_{z^2}
$Ni^+(CH_4)$	η^2 $C_{2v}(x)$ $^2A_2$	0.0935	0.0044	0.0029	0.0012	1.0276	1.9943	2.0000	1.9668	1.9813
	η^2 $C_{2v}(z)$ $^2A_2$	0.1337	0.0014	0.0031	0.0046	1.0000	1.9952	1.9921	1.9975	1.9201
$Ni^+(CH_4)_2$	η^2 $D_{2h}(x)$ $^2B_{1g}$	0.2440	0.0093	0.0045	0.0015	1.0609	1.9900	1.9999	1.9279	1.9658
	η^2 $D_{2h}(z)$ $^2B_{1g}$	0.2925	0.0019	0.0044	0.0091	1.0000	1.9921	1.9829	1.9963	1.8589
$Ni^+(CH_4)_3$	η^2 $C_{2v}(x)$ $^2A_1$	0.1726	0.0095	0.0064	0.0042	1.9915	1.9848	1.9934	1.0595	1.9433
	η^2 $C_{2v}(x)$ $^2A_2$	0.1807	0.0081	0.0090	0.0031	1.0687	1.9919	1.9912	1.9821	1.9557
	η^2 $C_{2v}(z)$ $^2A_2$[a]	0.2106	0.0047	0.0094	0.0058	1.0527	1.9976	1.9910	1.9357	1.9784
	η^2 $C_{2v}(z)$ $^2A_2$[b]	0.1545	0.0044	0.0081	0.0073	1.0326	1.9902	1.9913	1.9684	1.9863
$Ni^+(CH_4)_4$	η^2 $D_{4h}(z)$ $^2B_{2g}$	0.1752	0.0105	0.0105	0.0041	1.9932	1.9892	1.9892	1.0848	1.9545
	η^2 C_s $^2A^{11}$	0.1477	0.0101	0.0065	0.0082	1.9868	1.0546	1.9904	1.9775	1.9901
$Ni^+(CH_4)_5$	η^2 $C_{2v}(z)$ $^2A_1$	0.1712	0.0112	0.0112	0.0050	1.9932	1.9890	1.9888	1.0838	1.9571
$Ni^+(CH_4)_6$	η^2 $D_{2h}(z)$ ^2A_g	0.1691	0.0057	0.0117	0.0118	1.9892	1.9888	1.9932	1.7359	1.3050

[a]Outer shell structure [see Fig. 6(c)].
[b]Inner shell structure [see Fig. 6(d)].

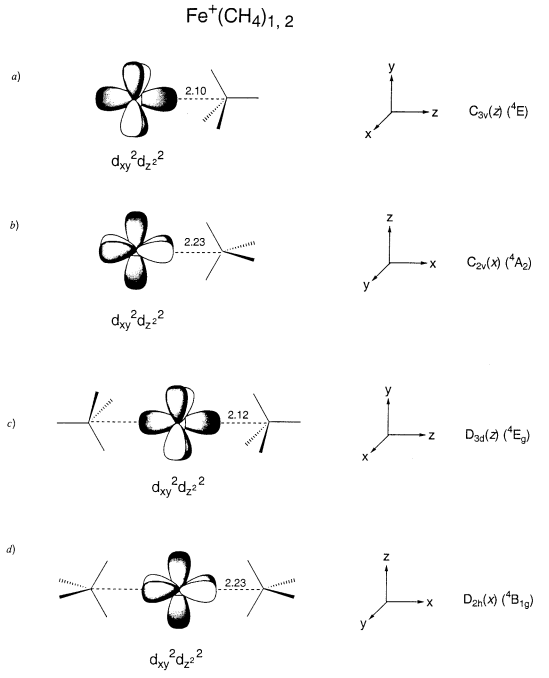

Fig. 3. Structures and states predicted by theory for the lowest energy structures of $Fe^+(CH_4)$ and $Fe^+(CH_4)_2$. Orbitals important for the bonding are shown as are the coordinate systems. For each of the state listing the principal bonding axis is given.

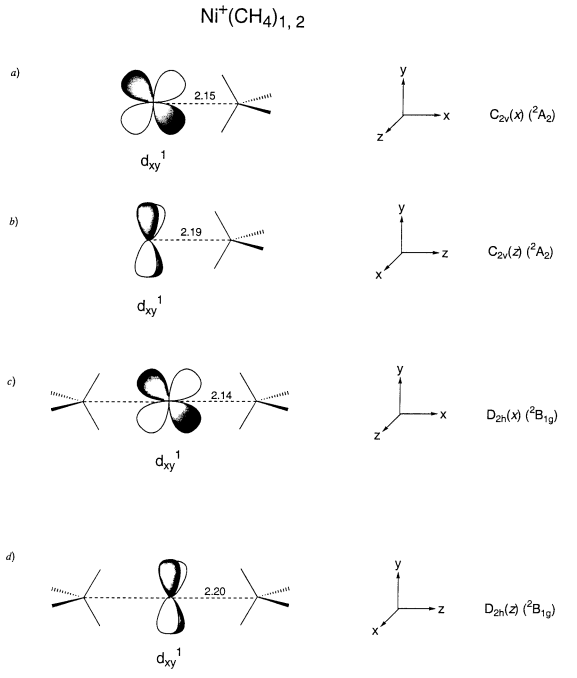

Fig. 4. Structures and states predicted by theory for the lowest energy structures of $Ni^+(CH_4)$ and $Ni^+(CH_4)_2$). Orbitals important for the bonding are shown.

following section we will discuss the systems in a pairwise manner, since experiment indicates this is how the bonding varies.

5. M^+CH_4 and $M^+(CH_4)_2$

5.1. M^+CH_4

A linear fit to the ΔG_T^0 versus temperature data (Fig. 1) for the first Fe^+–CH_4 association gives ΔH_T^0 and ΔS_T^0 values of −18.3 kcal/mol and −20.6 cal/(mol K), respectively (Table 1). The resulting bond energy (ΔH_0^0) from the statistical mechanical fit to the data is 17.5 kcal/mol (Table 1). An analogous ΔG_T^0 versus temperature plot for Ni^+–CH_4 association reaction is shown in Fig. 2. The ΔH_T^0 and ΔS_T^0 values were measured to be −26.8 kcal/mol and −20.5 cal/(mol K), respectively (Table 2). The resulting bond energy ($-\Delta H_0^0$) is 24.9 kcal/mol (Table 2).

For the second $Fe^+(CH_4)$–CH_4 association, the experiment gives ΔH_T^0 and ΔS_T^0 values of −25.9 kcal/mol and −28.6 cal/(mol K), respectively (Table 1). The resulting bond energy (ΔH_0^0) from the statistical mechanical fit to the data is 26.0 kcal/mol (Table 1). An analogous ΔG_T^0 versus temperature plot for $Ni^+(CH_4)$–CH_4 association reaction is shown in Fig. 2. The ΔH_T^0 and ΔS_T^0 values were measured to be −26.8 kcal/mol and −28.2 cal/(mol K), respectively (Table 2). The resulting bond energy ($-\Delta H_0^0$) is 26.5 kcal/mol (Table 2).

It is well known that the transition metal ions tend to ligate to inert species with a $3d^n$, instead of a $3d^{n-1}\,4s^1$ core electron configuration, to reduce the metal/ligand repulsion. Co^+ and Ni^+ are d^n ground state ions but Fe^+ has a $^6D(3d^6\,4s^1)$ ground state and the first excited state, $^4F(3d^7)$, lies 5.7 kcal/mol higher in energy. Of interest is whether the Fe^+ ion core changes both configuration and spin on clustering with the first CH_4 ligand. Schultz and Armentrout [14] concluded the Fe^+ core was unchanged on clustering

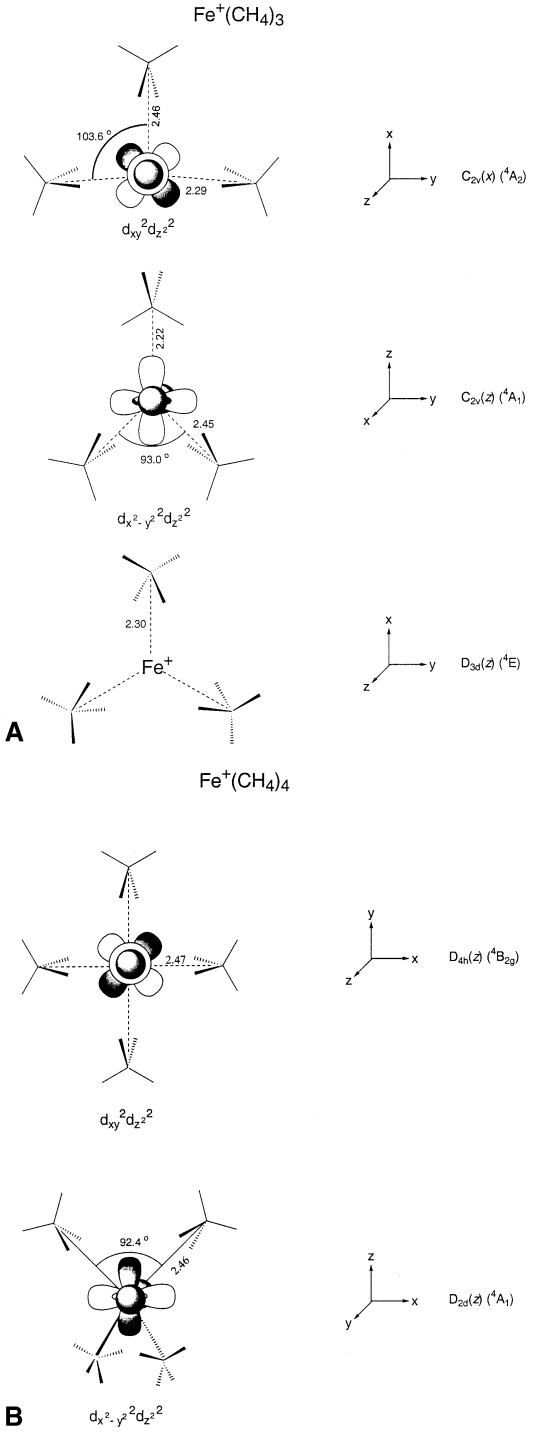

Fig. 5. Structures and states predicted by theory for the lowest energy structures of $Fe^+(CH_4)_3$ and $Fe^+(CH_4)_4$. Orbitals important for the bonding are shown.

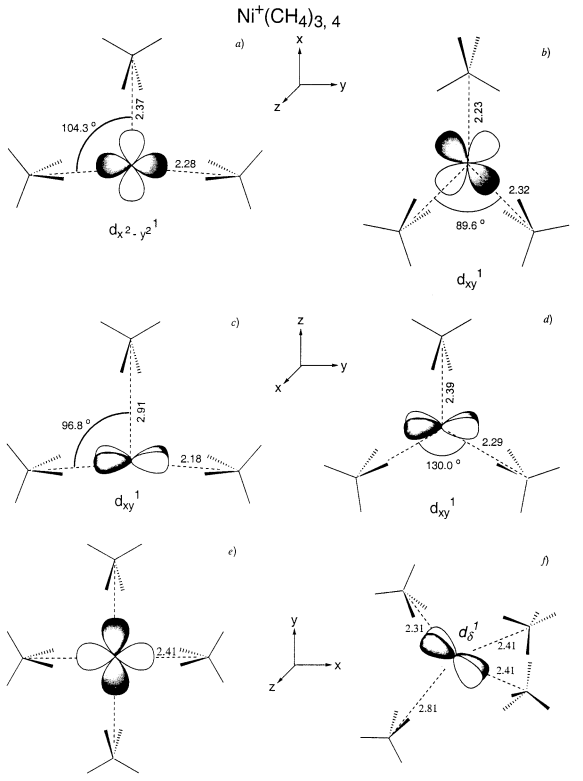

Fig. 6. Structures and states predicted by theory for the lowest energy structures of $Ni^+(CH_4)_3$ and $Ni^+(CH_4)_4$. Orbitals important for the bonding are shown.

the first CH_4 and remained a sextet but changed to a quartet on adding the second CH_4.

Table 5 summarizes the experimental and theoretical BDEs (ΔH_0^0) for reactions $M^+(CH_4)_{n-1} + CH_4 \rightleftharpoons M^+(CH_4)_n$ for $n = 1$–6, where $M^+ = Fe^+$, Co^+, and Ni^+. Co^+ and Ni^+ both have $3d^n$ ground states. The experimental BDE (ΔH_0^0) show that for Co^+ and Ni^+ the first methane is bound about 2 kcal/mol weaker than the second one, an effect due to the partial 3*d*/4*s* hybridization to reduce the metal to ligand repulsion [11]. In contrast, for Fe^+ the BDE (ΔH_0^0) for the first adduct is smaller than the second one by 8.5 kcal/mol. This unusually low binding energy may well be due to a change of spin state on clustering the first CH_4 requiring a promotion energy of 5.7 kcal/mol for the Fe^+ core. Our theoretical calculations give a diabatic BDE (ΔH_0^0) of 21.2 kcal/mol to the $3d^7$ asymptote. By subtracting the 5.7

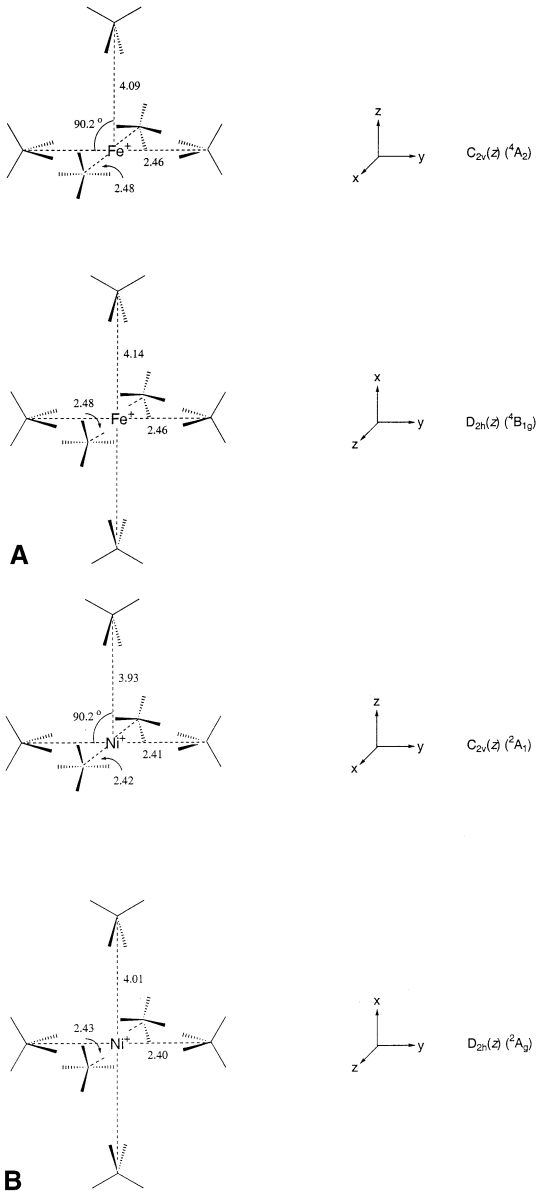

Fig. 7. Structures and states predicted by theory for the lowest energy structures of $Fe^+(CH_4)_{5,6}$ and $Ni^+(CH_4)_{5,6}$.

kcal/mol promotion energy, theory gives an adiabatic BDE (ΔH_0^0) of 15.5 kcal/mol (Table 3). If the $d^n/d^{n-1}\,s^1$ energy separation calibration is further considered, a BDE (ΔH_0^0) of 16.7 kcal/mol is obtained. Perry carried out modified coupled pair functional (MCPF) level calculation and obtained a BDE (D_e) of 15.7 kcal/mol [27], which is in good agreement with our current DFT calculation. This supports the proposition that a spin change takes place in the Fe^+ core on clustering to the first methane.

We also explored the BDE for the sextet high spin state. Theory indicates ground sextet spin state has a BDE (ΔH_0^0) of 9.7 kcal/mol with the $d^n/d^{n-1}\,s^1$ energy splitting calibration, and 10.4 kcal/mol without. Perry calculated a BDE (D_e) of 9.1 kcal/mol for the sextet, which again is in good agreement with our calculation. The guided ion beam experiment performed by Schultz and Armentrout gave a BDE of 13.7 kcal/mol for the first adduct (Table 1). They ascribed the low binding energy of this adduct to the high spin sextet state of Fe^+ in the cluster reasoning that the 4*s* electron is highly repulsive and will lower the BDE significantly. The BDE for the second adduct they measured is 23.3 kcal/mol (Table 1), which is comparable to our current measurement of 26.0 kcal/mol. Such a high BDE certainly cannot be due to the high spin Fe^+ core. Therefore, they claimed the sextet to quartet spin change takes place while Fe^+ ($d^6\,s^1$)CH_4 is clustering to the second methane. It is hard to distinguish when the spin change takes place in a collision-induced dissociation (CID) experiment. However, this dilemma can be clarified by the gas phase equilibrium experiment. For the following gas phase reaction

$$Fe^+(d^7)(CH_4)_2 \rightleftharpoons Fe^+(CH_4) + CH_4$$

the second cluster must have a d^7 electron configuration on the Fe^+ core for reasons just given. As equilibrium is approached between the first and second adducts, the $Fe^+(CH_4)$ adduct will eventually be dominated by $Fe^+(d^7)(CH_4)$ since it would be energetically unfavorable to form $Fe^+(d^6\,s^1)(CH_4)$. Therefore, the BDE we measured for the first association reaction in our equilibrium experiment is for the quartet species. This interpretation is supported by our DFT calculation and Perry's MCPF calculations. Finally if the spin change happens during clustering to the second methane, the diabatic BDE will be as high as 31.7 kcal/mol, a completely unrealistic value.

If the spin change is slow, relative to the collision rate, the addition of the first CH_4 to Fe^+ (^6D) should

Table 5
Experimental and theoretical BDE ($-\Delta H_0^0$) for reactions $M^+ (CH_4)_{n-1} + CH_4 \rightleftharpoons M^+ (CH_4)_n$ for $n = 1$–6, where $M^+ = Fe^+$, Co^+, and Ni^+

	Experiment			Theory		
n	Fe^+	Co^+	Ni^+	Fe^+	Co^+	Ni^+
1	17.5	23.1	24.9	15.5 (C_{3v})	22.9 (C_{2v})	23.9 (C_{2v})
2	26.0	25.3	26.5	21.5 (D_{3d})	22.1 (D_{2h})	22.9 (D_{2h})
3	5.2	7.3	9.3	4.0 (C_{2v})	4.6 (C_{2v})	7.4 (C_{2v})
4	4.9	5.2	5.5	3.0 (D_{4h})	2.2 (D_{2h})	3.7 (D_{4h})
5	~2	~2	~2	0.5 (C_{2v})	0.7 (C_{2v})	0.5 (C_{2v})
6	~2	~2	~2	0.2 (D_{2h})	0.3 (D_{2h})	0.4 (D_{2h})

be slow to come into equilibrium. To test this possibility, we varied the drift time from 0.15 to 2 ms. The variation of the Fe^+CH_4/Fe^+ observed ratios were within the experimental fluctuation. Hence, the sextet to quartet spin change must occur efficiently.

Various electron configurations and geometries will be explored theoretically for $M^+ (CH_4)_n$ adducts in this article. In order to be able to analyze the NBO population directly, we utilize the normal *d* orbital notation, using d_{z^2}, instead of d_{x^2} or d_{y^2} to represents a d_σ orbital. As a consequence, the *z* axis does not always represent the principal axis, but does give the d_σ orientation. We use molecular term symbols from character tables directly even though the principal axis is other than the *z* axis. Consequently we indicate the principal axis in addition to the molecular point group.

The DFT calculation with a Wachters(*f*)/6-31G(*d*, *p*) basis set indicates the first CH_4 ligand binds side on to Fe^+ in an η^3 configuration (Fig. 3). Choosing the *z* axis as the bonding axis, the $C_{3v}(z)$ ^4E ground state, with slightly distorted C_{3v} symmetry, has an electron configuration on Fe^+ of

$$d^1_{x^2-y^2}\, d^1_{xz}\, d^1_{yz}\, d^2_{xy}\, d^2_{z^2} \text{ or } d^1_{xy}\, d^1_{xz}\, d^1_{yz}\, d^2_{x^2-y^2}\, d^2_{z^2}$$

which retains the low energy ^4F state for the metal center. The calculated Fe^+–C bond length is 2.10 Å. For Ni^+, the calculation predicts that the CH_4 ligand binds side on to Ni^+ in an η^2 configuration (Fig. 4). The calculated Ni^+–C bond length is 2.15 Å. Choosing the *x* axis as the bonding axis and *z* axis perpendicular to the molecular plane, the $C_{2v}(x)$ $^2A_2$ ground state electron configuration of Ni^+ is

$$d^2_{x^2-y^2}\, d^2_{xz}\, d^2_{yz}\, d^2_{z^2}\, d^1_{xy}$$

which again retains the low energy ^2D state for the metal center.

A Mulliken population analysis shows there is 0.38 and 0.42 electron charge transfer from CH_4 into the half-filled 3*d*, and empty 4*s* and 4*p* orbitals on Fe^+ and Ni^+, respectively. The primary covalent interactions, as determined from NBO [28,29] population analyses (Tables 3 and 4), are donation from the a_1 symmetry orbital on CH_4 into the vacant 4*s* orbital in M^+. In addition, there is a small donation into the singly occupied d_{xz} and d_{yz} orbital on Fe^+ and into the singly occupied d_{xy} orbital (recall that *x* is the bond axis) on Ni^+. These charge transfer interactions result in a small elongation of the C–H bond (~0.03 Å) and reduction in the vibrational frequencies of the proximate C–H bonds by between 100 and 200 cm^{-1}. The 4*s* orbital also (partially) hybridizes with the on-axis doubly occupied d_{z^2} orbital in Fe^+ and the $d_{x^2-y^2}$ orbital (*x* is the bond axis for Ni^+CH_4 adduct) on Ni^+ generating two positive bonding effects: first, reduction of Pauli repulsion by shifting electron density off-axis and second improving overlap with the a_1 orbital on CH_4 by elongating the 4*s* orbital along the bond axis [30]. The NBO population shows a d_{z^2} occupancy of 1.8407 for Fe^+ and a $d_{x^2} - y^2$ occupancy of 1.9668 for Ni^+. Because the *d* orbitals contract with respect to the *s* orbitals with increasing *Z* for each transition row and the propensity for *s/d* hybridization increases as the radial extent of these orbitals becomes more similar. *s/d* hybridization is

therefore more favorable for early first row metals than for late first row metals.

Two η^2 quartet states, $C_{2v}(x)$ ($^4A_2$) and $C_{2v}(z)$ ($^4A_1$), were explored for iron. The calculated BDE ($-\Delta H_0^0$) is 15.1 kcal/mol for $C_{2v}(x)$ $^4A_2$ state, which is only 0.4 kcal/mol lower in binding energy than the $C_{3v}(z)$ (^4E) ground state. The bond distance was found to be 2.23 Å, 0.13 Å longer than the $C_{3v}(z)$ (^4E) ground state. Choosing the x axis as the bonding axis, the electron configuration of the $C_{2v}(x)$ $^4A_2$ state is

$$d^1_{x^2-y^2}\, d^1_{xz}\, d^1_{yz}\, d^2_{xy}\, d^2_{z^2}$$

where the doubly occupied d_{xy} orbital bridges the two proximate hydrogens to avoid repulsion. The d_{z^2} orbital is doubly occupied to maintain the pure atomic coupling of the Fe^+ core.

The $C_{2v}(z)$ ($^4A_1$) state has a d electron configuration of

$$d^1_{xy}\, d^1_{xz}\, d^1_{yz}\, d^2_{x^2-y^2}\, d^2_{z^2}$$

The doubly occupied d_{z^2} orbital is oriented on the bond axis and increases on-axis repulsion to the ligand, decreasing the bond energy by 1.4 kcal/mol relative to $C_{2v}(x)$ ($^4A_2$) state. It is surprising that the Fe^+–C bond length is not elongated relative to the $C_{2v}(x)$ ($^4A_2$) state. The analyses of the NBO population (Table 3) shows that the d_{z^2}/s hybridization in the $C_{2v}(z)$ ($^4A_1$) state is nearly twice as great as in the $C_{2v}(x)$ ($^4A_2$) state. This hybridization helps reduce the on-axis repulsion and therefore helps shorten the bond distance. The calculated BDE is 13.7 kcal/mol for this state.

As mentioned previously, the high spin sextet ground state also has C_{3v} symmetry. The electron configuration of Fe^+ in this $C_{3v}(z)$ ^6E state is

$$d^1_{xy}\, d^1_{xz}\, d^1_{yz}\, d^1_{z^2}\, d^2_{x^2-y^2}\, s^1$$

The Fe^+–C bond length is 2.52 Å, significantly longer than the low spin states. Another high spin $C_{2v}(z)$ ($^6A_1$) state with a z principal axis has the electron configuration of

$$d^1_{xy}\, d^1_{xz}\, d^1_{yz}\, d^1_{z^2}\, d^2_{x^2-y^2}\, s^1$$

The BDE is 9.5 kcal/mol. The bond length is 2.65 Å. For both the low and high spin states, the C_{2v} structures are slightly less favorable compared to the C_{3v} structure for $Fe^+(CH_4)$ species.

For nickel, the $C_{2v}(x)(^2A_2)$ ground state (Fig. 4) has a Ni^+–C bond distance of 2.15 Å. A second η^2 state, $C_{2v}(z)$ ($^2A_2$), has the d_{z^2} orbital oriented along the bond axis of Ni^+ and CH_4. The singly occupied d_{xy} orbital lies perpendicular to the bond axis, which results in an electron configuration of Ni^+ as

$$d^2_{x^2-y^2}\, d^2_{xz}\, d^2_{yz}\, d^2_{z^2}\, d^1_{xy}$$

For this state, the doubly occupied d_{yz} orbital is directed toward the proximate pair of hydrogen in methane, causing both more repulsion between metal and ligands and loss of the back donation from the η^2 hydrogens. One might hope to evaluate the difference of repulsion and donation between the singly and the doubly occupied d_π [d_{yz} in the $C_{2y}(z)$ $^2A_2$ state and d_{xy} in the $C_{2v}(x)$ $^2A_2$ state) orbitals by comparing the $C_{2v}(x)$ $^2A_2$ and the $C_{2v}(z)$ $^2A_2$ states. However, the prior reorientation also causes other changes in the bonding features. One aspect is that the extent of s/d hybridization is different. The d_{z^2} orbital in the $C_{2v}(z)$ $^2A_2$ state has a higher electron density than the $d_{x^2\text{-}y^2}$ orbital in the $C_{2v}(x)$ $^2A_2$ state along the bond axis which results in a more extensive hybridization to the empty 4_s orbital on Ni^+ (to reduce repulsion). Consequently, the more extensive s/d hybridization costs more promotion energy. The calculated $^2D(3d^9) \rightarrow {}^4F(3d^8\ 4s^1)$ separation with the Wachters(f)6-31G(d, p) basis is 26.6 kcal/mol. Based on the NBO population, the $C_{2v}(z)$ $^2A_2$ state needs about 1 kcal/mol more promotion energy than the $C_{2v}(x)$ $^2A_2$ state to hybridize the on-axis $3d$ orbital with the $4s$ orbital. For simplicity, if the difference of on-axis d_σ repulsion and other effects are negligible, the increase in d_π repulsion and reduced back donation will cause a slightly more than 2 kcal/mol decrease in binding energy for the Ni^+–CH_4 system. The net effect is a slightly elongated(0.04 Å) bond length and a decrease in BDE of 1.4 kcal/mol.

An η^3 C_{3v} structure was also explored. Due to the Jahn-Teller effect, the molecular orbitals only have C_s

symmetry. Unlike Fe^+ (CH_4), the η^3 C_{3v} configuration is less favorable than the $\eta^2 C_{2v}$ vee structure. The binding energy is 0.9 kcal/mol lower than the $C_{2v}(x)$ $(^2A_2)$ ground state. The calculated bond distance is 2.09 Å. The only singly occupied *d* orbital orients to one of the proximate hydrogens in methane. After lifting the symmetry constraint, the η^3 C_{3v} structure eventually converged to the $C_{2v}(x)$ $(^2A_2)$ state.

5.2. $M^+(CH_4)_2$

The ground state for Fe^+ $(CH_4)_2$ was found to be η^3 $D_{3d}(z)$ (^4E_g) from the DFT calculation. The electron configuration of Fe^+ is

$$d^1_{x^2-y^2}\, d^1_{xz}\, d^1_{yz}\, d^2_{xy}\, d^2_{z^2}$$

Again, the d_{z^2} orbital is oriented along the bond axis. The calculated BDE is 21.5 kcal/mol. The Fe^+–CH_4 bond distance is 2.12 Å, slightly longer than the first cluster. Two low spin quartet states with D_{2h} symmetry, corresponding to the quartet C_{2v} structures in first adduct, were also considered. For the $D_{2h}(x)$ $(^4B_{1g})$ state, the valence electron configuration of Fe^+ is

$$d^1_{x^2-y^2}\, d^1_{xz}\, d^1_{yz}\, d^2_{xy}\, d^2_{z^2}$$

The BDE is 19.6 kcal/mol and the bond distance is 2.23 Å. The $D_{2h}(z)$ (^4A_g) state with *z* principal axis has the valence electron configuration as

$$d^1_{xz}\, d^1_{yz}\, d^1_{xy}\, d^2_{x^2-y^2}\, d^2_{z^2}$$

The BDE is 19.0 kcal/mol and the bond distance is 2.23 Å.

For nickel, a $D_{2h}(x)$ $^2B_{1g}$ ground state is obtained with the second methane directly opposite the first on the Ni^+ center. Choosing the *x* axis as the bonding axis, the $D_{2h}(x)$ $^2B_{1\ g}$ ground state (Fig. 4) electron configuration of Ni^+ is

$$d^2_{x^2-y^2}\, d^2_{xz}\, d^2_{yz}\, d^2_{z^2}\, d^1_{xy}$$

A bond dissociation energy of 22.9 kcal/mol is calculated in good agreement with experiment. It is worth noticing that the experimental BDE is 1.6 kcal/mol larger for the second CH_4 ligand than for the first whereas theory predicts a slightly lower BDE for the second *vs* the first. This is probably a result of an overestimation of the first BDE by the DFT method, something that we have previously observed [31].

The $D_{2h}(z)$ $^2B_{1g}$ state (Fig. 4), which corresponds to the $C_{2v}(z)$ $^2A_2$ state in the first cluster, has a BDE 2.5 kcal/mol smaller than the $D_{2h}(x)$ $^2B_{1g}$ ground state.

For Fe^+, Co^+, and Ni^+, the BDE of the second adduct is experimentally found to be about 2.5 kcal/mol higher than the first one (for Fe^+, the diabatic BDE is 23.2 kcal/mol), which is shown in Table 5. The DFT calculations usually overestimate the first BDE. For Fe^+, Co^+, to Ni^+, the BDEs tend to increase monotonically across the row, which is due to an increase of charge transfer. However, for Fe^+, since the ground states have η^3 configurations, relatively higher BDEs are obtained, an effect well reproduced by the DFT calculations.

6. M^+ $(CH_4)_3$ and $M^+(CH_4)_4$

A linear fit to the ΔG^0_T versus temperature data (Fig. 1) for the third Fe^+–CH_4 association gives ΔH^0_r and ΔS^0_r values of −5.6 kcal//mol and −22.5 cal/(mol K), respectively (Table 1). The resulting bond energy $(-\Delta H^0_0)$ from the statistical mechanical fit to the data is 5.2 kcal/mol (Table 1). An analogous ΔG^0_T versus temperature plot for Ni^+–CH_4 association reaction is shown in Fig. 2. T he ΔH^0_T and ΔS^0_T values were measured to be −8.4 kcal/mol and −18.5 cal/(mol K), respectively (Table 2). The resulting bond energy $(-\Delta H^0_0)$ is 9.3 kcal/mol (Table 2).

For the fourth Fe^+ $(CH_4)_3$–CH_4 association, the experiment gives ΔH^0_T of about −4.7 kcal/mol and the ΔS^0_T is estimated to be about −20 cal(mol K) (Table 2). These parameters could not be obtained as accurately as those for the first three CH_4 ligands due to a persistent impurity. A very thorough study of the Co^+ system indicates the impurity is almost certainly O_2. The resulting bond energy $(-\Delta H^0_0)$ from the statistical mechanical fit to the data is 4.9 kcal/mol (Table 1). An analogous ΔG^0_r versus temperature plot for

$Ni^+(CH_4)_3$–CH_4 association reac tion is shown in Fig. 2. The ΔH_T^0 and ΔS_T^0 values were estimated to be −5.5 kcal/mol and −20 cal/(m ol K), respectively (Table 2). Again the persistent impurity made a more accurate measurement impossible. The resulting bond energy ($-\Delta H_0^0$) is 5.5 kcal/mol (Table 2).

As expected the calculation shows a significantly weaker bond energy for the third and the fourth CH_4 ligands. For $Fe^+(CH_4)_3$, The calculated BDE for the $C_{2v}(x)$ ($^4A_2$ ground state (Fig. 5) is 4.0 kcal/mol (Table 1). The doubly occupied d_{xy} orbital bridges all three methanes and the other doubly occupied d_{z^2} orbital is perpendicular to the molecular plane, resulting in two short bonds of 2.29 Å and one longer bond of 2.46 Å.

The second structure we explored has $C_{2v}(z)$ ($^4A_1$) symmetry. The BDE calculated wit h a DZVP/6-31G(*d, p*) basis is 2.0 kcal/mol lower than the $C_{2v}(x)$ ($^4A_2$) state. For this state, the doubly occupied d_{z^2} orbital points to one CH_4 and the other doubly occupied *d* orbital is $d_{x^2\text{-}y^2}$.

A third structure is trigonal with $D_3(z)$ symmetry with the CH_4 ligands rotated 31.5 ° around the Fe^+–C bond axis from a "planar" D_{3h} structure. In this instance, the electron configuration is

$$e_1(d_{x^2-y^2} - d_{xz})^2 e_1(d_{xy} + d_{yz})^2 e_2(d_{x^2-y^2} + d_{xz})^1 e_2(d_{xy} - d_{yz})^1 a_1(d_{z^2})^1$$

The *z* axis is the principal rotation axis perpendicular to the plane containing the three CH_4 ligands. Two of singly occupied orbitals, $e_2(d_{x^2-y^2} + d_{xz})^1$ and $e_2(d_{xy}-d_{yz})^1$ are oriented to accept electron density from a pair of hydrogens on one of the CH_4 ligands while the doubly occupied orbitals are at right angles to minimize repulsion. Some *s/d* hybridization occurs with the d_{z^2} orbital to minimize repulsion.

For $Ni^+(CH_4)_3$, our density functional theory (DFT) calculations found two configurations with essentially the same energy (Table 2). The first is a near T-shape with the third CH_4 ligand approaching at 90 ° to the line of centers of the η^2 C_{2v} $Ni^+(CH_4)_2$ structure. By choosing the *x* a xis as the principal axis, the singly occupied $d_{x^2\text{-}y^2}$ orbital has three lobes oriented toward the CH_4 ligands and the d_{z^2} orbital is perpendicular to the molecular plane. This results in a $C_{2v}(x)$ $^2A_1$ state (Fig. 6). The clustering of the third CH_4 to Ni^+ is significantly different than for Co^+. In the cobalt case, the association of the third CH_4 is impeded by *s/d* hybridization, which results in a T-shape structure with two short Co^+–C bonds (2.23 Å) and one long bond (2.57 Å). However, for the $Ni^+(CH_4)_3$ ground state $C_{2v}(x)$ $^2A_1$, the most repulsive *d* orbital is the doubly occupied d_{yz} orbital, which hybridizes with the empty ^4S orbital and does not hinder the clustering of the third CH_4 in the *x* direction. As a result, the T-shape structure has two Ni^+–C bonds of 2.28 Å and one slightly longer (2.37 Å). These three bonds are nearly identical. The calculated bond energy ($-\Delta H_0^0$) is 7.4 kcal/mol, which is in good agreement with the experimental, BDE, 9.3 kcal/mol. Notice that the $D_{2h}(x)$ ($^2B_{1g}$) ground state of thee second cluster has the singly occupied d_{xy} orbital facing four proximate hydrogens from the ligands. To form the third cluster from this state a rearrangement of the methanes around Ni^+ core ion is required.

The second bound structure, $^2A_2$, is trigonal with $C_{2v}(x)$ symmetry (Fig.6). The two identical methanes ligate to the two lobes of the d_{xy} orbital with a bond length of 2.32 Å. The third methane, therefore, orients to the other two lobes of this orbital with a bond length of 2.23 Å. This relatively strong bond gets most of the benefit of ligand to metal donation. The *s/d* hybridization only impedes clustering perpendicular to the molecular plane, and therefore, does not interfere with the bonding of the other two methanes.

We also considered the structure which inherits the electron configuration from the $D_{2h}(x)$ ($^2B_{1g}$) ground state from the second cluster, resulting in a $C_{2v}(z)$ $^2A_2$ state [Fig. 6(*c*)]. Under this orientation of methanes, the first two methanes provide most of the electron donation to Ni^+ ion. The clustering of the third methane is impeded by the doubly occupied d_{z^2} orbital and the *s/d* hybridization mention above. This results in a much longer bond distance, 2.91 Å, for the third methane. The calculated bond dissociation energy (D_e) is 2.0 kcal/mol, which is significantly lower than the experimental value. Because this bond is so long we had to carefully account for basis set superposition energy (BSSE) to ensure the methane was really

bound. The calculated BSSE is 0.2 kcal/mol, which ensures the validity of bonding. From the analysis of the electron population, there is almost no covalent interaction between this methane and Ni^+ core ion. The bonding is essentially only electrostatic attraction.

Under the same orientation, another bound $C_{2v}(z)$ $^2A_2$ state was found to have the trigonal structure [Fig. 6(d)], which has two short Ni^+–C bonds (2.29 Å) and one longer Ni^+–C bonds (2.39 Å). The calculated bond dissociation energy (D_e) is 1.9 kcal/mol. This configuration loses some of the covalent bond character but partially compensates by electrostatic attraction.

For $Fe^+(CH_4)_4$, the ground state was found to be $D_{4h}(z)$ ($^4B_{2g}$) with a BDE of 3.0 kcal/mol. The two doubly occupied *d* orbitals are shown in Fig 5. This adduct inherits the electronic configuration from the ground state of the third cluster. The bond distance for the four equivalent bonds is of 2.47 Å. The stationary energy for a $D_{zd}(z)$ ($^4A_1$) state is 1.4 kcal/mol lower than the $D_{4h}(z)$ ($^4B_{2g}$) state. The BDE, after vibrational zero point energy (ZPE) calibration, is 2.8 kcal/mol, near degenerated to the $D_{4h}(z)$ ($^4B_{2g}$)state.

For $Ni^+(CH_4)_4$, our DFT calculations found the ground state to be $^2B_{2g}$ with $D_{4h}(z)$ symmetry (Fig.6). The singly occupied $d_{x^2-y^2}$ orbital lies in the molecular plane and points to the four CH_4ligands. The Ni^+–C bond length is 2.41 Å. The calculated bond energy is 3.7 kcal/mol. A cluster with C_s symmetry at quasitetrahedral geometry was also considered. It has one short bond (2.31 Å), two intermediate (2.41 Å) and one long bond (2.81 Å) (Fig. 6). The singly occupied orbital is oriented to minimize repulsion. The furthest CH_4 ligand has a doubly occupied d_σ orbital pointed directly toward it. This structure has a very small BDE for loss of a CH_4 ligand.

We are not able to measure accurately the bond dissociation energy in our equilibrium experiment for $n = 4$. The peak *m/z* 122 [nominally Ni^+ $(CH_4)_4$] is observed in our experiments. However, the species is formed irreversibly in the temperature range 150–270 K, which is probably due to a persistent impurity, possibly O_2, in our system. For temperatures under 120 K, good equilibra between reactants and products are observed. However, due to significant collision induced dissociation after the reaction cell, we are still unable to get a temperature versus ΔG_T plot in the temperature range under 120 K. The only temperature we are able to obtain a good temperature *vs* ΔG_T plot is $T = 140$ K. At $T = 140$ K, the measured $\Delta/G_T = -2.7$ kcal/mol. The slope, ΔS, is estimated to be -20 cal/(mol K). Therefore, we postulate the ΔH_T^0 to be about 5.5 kcal/mol. For such a low temperature, the ΔH_T^0 value will be very close to the ΔH_0^0value. The calculated binding energy of 3.7 kcal/mol is somewhat smaller than experiment, but that is not unexpected for a molecule of this size at this level of theory. The experimental BDE rises from iron to nickel by about 2 kcal/mol for binding the third CH_4 ligand. Theory reflects this tendency well. For the fourth ligand, the BDEs are nearly the same, but still increase slightly from iron to nickel. Theory is in good agreement with experiment for Fe^+ and Ni^+ but does not do as well for cobalt.

The guided ion beam results are much different than our equilibrium studies for $n = 3$ and $n = 4$ in the iron system (See Table 1). for $n = 3$, the guided ion beam results indicate the BDE is 23.6 kcal/mol, or an *increase* of 0.3 kcal/mol over $n = 2$. By contrast, our equilibrium results indicate the BDE for $n = 3$ is 5.2 kcal/mol, or a *decrease* of 20.8 kcal/mol. For $n = 4$, we also obtain a relatively weak BDE of 4.9 kcal/mol whereas a value of 17.6 kcal/mol is obtained by the guided ion beam method. Schultz and Armentrout [14] suggest the Fe^+ core in $Fe^+(CH_4)_3$ retains a quartet spin stat but do not speculate on why the BDE is so high. In the same work they measure the BDE of $Fe^+(H_2O)_3$ to be 18.2 kcl/mol, or 21.1 kcal/mol less than the BDE for $Fe^+(H_2O)_2$. This kind of large drop in BDE from $n = 2$ to $n = 3$ has been observed for all late first row metal ions for $L = H_2$. The reason is there are no vacant *d* orbital on these metals and only two favorable locations for attachment of nonoxidizing ligands. Promotion energies to low spin states with more favorable orbital configurations are generally prohibitively high. Theory supports this view and indicates attachment of a third CH_4 ligand (or H_2 ligand) should result in a strongly reduced BDE. The only conclusion we can make is the guided ion beam data for the dissociation of

$Fe^+(CH_4)_3$ to $Fe^+(CH_4)_2$ + C H_4 must somehow be in error. Based on our careful studies on the Co^+/CH_4 system one possibility could be the presence of a significant O_2 impurity. In this instance the dissociation observed in the guided ion beam experiment would be

$$O_2Fe^+(CH_4) \xrightarrow{\text{CID}} O_2Fe^+ + CH_4 \quad (5)$$

which could well have a BDE of 23 kcal/mol.

Schultz and Armentrout[14] suggest a spin change from quartet to doublet may account for the drop in BDE for $n = 3$ and $n = 4$ in the iron system. Even if our suggestion given for the $n = 3$ case above is not correct, such a spin change is almost certainly not occurring. The lowest energy doublets state of Fe^+ is about 2 eV, or 46 kcal/mol, higher in energy than the Fe^+ ground state and about 40 kcal/mol above the ^4F first excited state with d^7 configuration. Hence, the observed diabatic dissociation energy would be about 57 kcal/mol, far too large for even the first CH_4 ligand. Our equilibrium value is ~5 kcal/mol for $n = 4$ which is supported by theoretical calculations. Again it appears there is a problem with the experimental guided ion beam value, and O_2 impurity might also be implicated.

7. $M^+(CH_4)_5$ and $M^+(CH_4)_6$

For $Fe^+(CH_4)_5$, the ΔH_T^0 and ΔS_T^0 were estimated to be about −2 kcal/mol and −10 cal/(mol K) (Table 1). The ΔH_T^0 was measured at temperature range 80–110 K. For $Ni^+(CH_4)_5$, the ΔH_T^0 and ΔS_T^0 were also estimated to be about −2 kcal/mol and −10 cal/(mol K) (Table 2). The ΔH_T^0 was measured at temperature range 80–140 K. For such low temperatures, ΔH_0^0 is expected to be very close to the ΔH_T^0 value. The small ΔS_T^0 value indicates that the fifth methane is in the second solvation shell for both metals.

For Fe^+, the DFT calculations show that the fifth methane approaches vertically to the molecular plane of $Fe^+(CH_4)_4$, resulting in a $C_{2v}(z)$ symmetry cluster. The $^4A_2$ ground state electron configuration of Fe^+ is

$$d^1_{x^2-y^2}\, d^1_{xz}\, d^1_{yz}\, d^2_{xy}\, d^2_{z^2}$$

A BDE of 0.5 kcal/mol is calculated. The Fe^+–C bond distance for the fifth methane is 4.09 Å, consistent with a second solvation shell.

For Ni^+, the DFT calculations show that the fifth methane also approaches vertically to the molecular plane of $Ni^+(CH_4)_4$. By choosing the x axis as the principal axis, the $C_{2v}(z)$—$^2A_1$ ground state electron configuration of Ni^+ is

$$d^2_{xy}\, d^2_{xz}\, d^2_{yz}\, d^2_{z^2}\, d^1_{x^2-y^2}$$

A bond dissociation energy of 0.5 kcal/mol is calculated, again in good agreement with experiment. The C_{axial}–Ni–$C_{equatorial}$ bond angle is 90.2° and the Ni^+–C bond length of the four equatorial methanes are 2.41 and 2.42 Å; or about the same as those in $Ni^+(CH_4)_4$. The NBO population shows that the d electron population of $Ni^+(CH_4)_5$ is very close to that of $Ni^+(CH_4)_4$ (Table 4). The bond length of the fifth methane approaching in the z direction is 3.93 Å. Analysis of the Mulliken charge population indicates there is almost no charge transfer between Ni^+ and the fifth methane. The results are consistent with a second solvation shell for the fifth CH_4 ligand.

For $Fe^+(CH_4)_6$, ΔG_T^0 is measured to be 1.2 kcal/mol at 80 K (Table 1). If we assume ΔS_T^0 to be about 10 cal/(mol K), we estimate a bond dissociation energy of 2.0 kcal/mol for the sixth methane.

For $Ni^+(CH_4)_6$, the ΔG_T^0 is also measured to be 1.2 kcal/mol at 80 K (Table 2). Again assuming ΔS_T^0 to be about 10 cal/(mol—K), we estimate a bond dissociation energy of 2.0 kcal/mol for the sixth methane.

The DFT calculations indicate a $^4B_{1g}$ ground state with $D_{2h}(z)$ symmetry for $Fe^+(CH_4)_6$. A bond dissociation energy of 0.2 kcal/mol is obtained. The axial Fe^+–C bond length is 4.14 Å and the equatorial Fe^+–C bond lengths are 2.46 and 2.48 Å. The charge on iron is +0.08. There is almost no charge transfer between Fe^+ and the $n = 5$ and $n = 6$ CH_4 ligands.

The DFT calculations indicate a ^2A_g ground with $D_{2h}(z)$ symmetry for $Ni^+(CH_4)_6$. A bond dissociation

energy of 0.4 kcal/mol is obtained. The axial Ni^+–C bond length is 4.01 A and the equatorial Ni^+–C bond lengths are 2.40 and 2.43 A. The charge on nickel is +0.06. There is no charge transfer between $n = 5$ and $n = 6$.

8. Conclusions

The sequential binding energies of CH_4 ligands to Fe^+ and Ni^+ are measured for $n = 1$–6. The binding energies decrease in a pairwise fashion from $n = 1, 2$ to $n = 5, 6$. Theory suggests the $n = 1, 2$ pair benefit from *s*/*d* hybridization that reduces Pauli repulsion and fosters sigma donation from the C–H bonds into partially filled orbitals on M^+. For the first two adducts, an η^3 structure is more favorable for Fe^+ but n^2 structures form the ground states for Co^+ and Ni^+. A spin change from ^6D ($3d^6 4s^1$) state to a ^4F ($3d^7$) state on the Fe^+ core occurs on addition of the first CH_4 ligand. Theory indicates a switch from η^3 to η^2 coordination for $Fe^+(CH_4)_3$, primarily to reduce Pauli repulsion. Theory also predicts the ground states of both $Fe^+(CH_4)_4$ and $Ni^+(CH_4)_4$ are pseudo planar with D_{4h} symmetry. Both experiment and theory suggest that both $Fe^+(CH_4)_{5,6}$ and $Ni^+(CH_4)_{5,6}$ are in the second solvation shell.

Acknowledgements

The support of the National Science Foundation under grant no. CHE-9729146 is gratefully acknowledged. One of the authors (M.T.B.) also wishes to thank Nico for 30 years of productive and enjoyable interactions, and for the inspiration his insight and boundless energy have given.

Reference

[1] J.C. Weisshaar, Acc. Chem. Res. 26 (1993) 213.
[2] B.A. Arndsten, R.G. Bergman, T.A. Mobley, T.H. Peterson, Acc. Chem. Res. 28 (1995) 154.
[3] Organometallic Ion Chemistry, B.S. Freiser (Ed.), Kluwer Academic, Dordrecht, The Netherlands, 1996.
[4] P. Kebarle, S.K. Searles, A. Zolla, J. Scarborough, M. Arshadi, J. Am. Chem. Soc. 89 (1967) 6393; A.M. Hogg, P. Kebarle, J. Chem. Phys. 43 (1965) 449.
[5] P.B. Armentrout, B.L. Kickel, Organometallic Ion Chemistry, B.S. Freiser (Ed.), Kluwer Academic, Dordrecht, The Netherlands, 1996.
[6] C.W. Bauschlicher, S.R. Langhoff, H. Partridge, Organometallic Ion Chemistry, B.S. Freiser (Ed.), Kluwer Academic, Dordrecht, The Netherlands, 1996.
[7] P.R. Kemper, P. Weis, M.T. Bowers, Chem. Phys. Lett. 293 (1998) 503, and reference therein.
[8] M.T. Bowers, P.R. Kemper, P.A.M. von Koppen, T. Wyttenbach, C.J. Carpenter, P. Weis, J. Gidden Energetics of Stable Molecules and Reaction Intermediates, M.E. Hinas da Piedade (Ed.), Kluwer Academic, Dordrecht, The Netherlands, 1999, pp. 235–258.
[9] P. Weis, P.R. Kemper, M.T. Bowers, J. Phys. Chem. A 101 (1997) 2809.
[10] P.A.M. van Koppen, J.E. Bushnell, P.R. Kemper, M.T. Bowers, J. Am. Chem. Soc. 117 (1995) 2098; P.A.M. van Koppen, J. Perry, P.R. Kemper, J.E. Bushnell, M.T. Bowers, Int. J. Mass Spectrom. 187 (1999) 989.
[11] Q. Zhang, P.R. Kemper, S.K. Shin, M.T. Bowers, Int. J. Mass. Spectrom., 284 (2001) 28.
[12] P.R. Kemper, J. Bushnell, P.A.M. van Koppen, M.T. Bowers, J. Phys. Chem. 97 (1993) 1810; C.L. Haynes, P.B. Armentrout, J.K. Perry, W.A. Goddard III, ibid. 99 (1995) 6340.
[13] C.J. Carpenter, P.A.M. van Koppen, M.T. Bowers, J. Perry, J. Am. Chem. Soc. 122 (2000) 392.
[14] R.H. Schultz, P.B. Armentrout, J. Phys. Chem. 97 (1993) 596.
[15] J.E. Bushnell, P.R. Kemper, P. Maitre, M.T. Bowers, J. Am. Chem. Soc. 116 (1994) 9710.
[16] P.R. Kemper, P. Weis, M.T. Bowers, Int. J. Mass. Spectrom. Ion Processes 160 (1997) 17.
[17] P.R. Kemper, M.T. Bowers, J. Am. Soc. Mass Spectra 1 (1990) 197.
[18] P.J. Stephens, F.J. Devlin, C.F. Chabalowski, M.J. Frisch, J. Phys. Chem. 98 (1994) 11623.
[19] A. Becke, J. Chem. Phys. 98 (1993) 5648.
[20] M.J. Frisch, G.W. Trucks, H.B. Schlegel, G.E. Scuseria, M.A. Robb, J.R. Cheeseman, V.G. Zakrzewski, J.A. Montgomery Jr., R.E. Stratmann, J.C. Burant, S. Dapprich, J.M. Millam, A.D. Daniels, K.N. Kudin, M.C. Strain, O. Farkas, J. Tomasi, V. Barone, M. Cossi, R. Cammi, B. Mennucci, C. Pomelli, C. Adamo, S. Clifford, J. Ochterski, G.A. Petersson, P.Y. Ayala, Q. Cui, K. Morokuma, D.K. Malick, A.D. Rabuck, K. Raghavachari, J.B. Foresman, J. Cioslowski, J.V. Ortiz, A.G. Baboul, B.B. Stefanov, G. Liu, A. Liashenko, P. Piskorz, I. Komaromi, R. Gomperts, R.L. Martin, D.J. Fox, T. Keith, M.A. Al-Laham, C.Y. Peng, A. Nanayakkara, C. Gonzalez, M. Challacombe, P.M.W. Gill, B. Johnson, W. Chen, M.W. Wong, J.L. Andres, C. Gonzalez, M. Head-Gordon, E.S. Replogle, J.A. Pople, Gaussian, Inc., Pittsburgh, PA, 1998.
[21] N. Godbout, D.R. Salahub, J. Andzelm, E. Wimmer, Can. J. Chem. 70 (1992) 560.
[22] A.J.H. Wachters, J. Chem. Phys. 52 (1970) 1033.
[23] C.W. Bauschlicher, Jr. S.R. Langhoff and L.A. Barnes, J. Chem. Phys. 91, 2399 (1989)

[24] C.E. Moore Atomic Energy Levels, Natl. Bureau of Standards (USA), Circ, 467, Washington, DC, 1949.
[25] M.C. Holthausen, W. Koch, Helv. Chim. Actal 79 (1996) 1939.
[26] (a) O. Gunnarson, R.O. Jones, Phys. Rev. B 31 (1985) 7588; (b) T. Ziegler, J. Li Can. J. Chem. 72 (1994) 783.
[27] J.K. Perry, Ph.D. thesis, California Institute of Technology, 1994.
[28] A.E. Reed, L.A. Curtis, F. Weinhold, Chem. Rev. 88 (1988) 899.
[29] We used the program in GAUSSIAN 98, [26].
[30] (a) C.W. Bauschlicher, H. Partridge, S.R. Langhoff, J. Chem. Phys. 91 (1989) 4733; (b) H. Patridge, C.W. Bauschlicher, S.R. Langhoff, J. Phys. Chem. 96 (1992) 5350; (c) C.W. Bauschlicher, H. Partridge, S.R. Langhoff, Chem. Phys. Lett. 165 (1990) 272.
[31] J.E. Bushnell, P. Maître, P.R. Kemper, M.T. Bowers, J. Chem. Phys. 106 (1997) 10153.